Оптический журнал

Физическая оптика

УДК 535.8; 537.8

Фильтр поверхностных плазмон-поляритонов на структуре металл–изолятор–металл, состоящий из двух оппозитных полуколец с различными радиусами

© 2017 г. Xia Liu**; Jinping Tian*,**; Rongcao Yang**

*Computer Center of Shanxi University, Taiyuan, P. R. China
**College of Physics and Electronics Engineering of Shanxi University, Taiyuan,P. R. China

Исследованы характеристики распространения возбужденных поверхностных плазмон-поляритонов в плазмонном фильтре при контролируемом изменении геометрических параметров волновода. Предлагаемый фильтр состоит из двух последовательных наноразмерных волноводов типа «металл–изолятор–металл» соединенных оппозитными, размещенными на верхней и нижней сторонах, концентрическими полукольцами с различными радиусами. Численный анализ показал, что длина волны, соответствующая «провалу» в спектре пропускания, сдвигается в длинноволновую сторону при увеличении радиуса полуколец, либо при увеличении показателя преломления изолятора. Поскольку возможность перестройки является важнейшей характеристикой фильтра, мы полагаем, что предложенная волноводная структура является перспективной для создания устройств нанофотоники.

Ключевые слова: *поверхностные плазмон-поляритоны, фильтр, спектр пропускания .*

UDC 535.8; 537.8

Surface plasmon polariton based metal-insulator-metal filter including two face to face concentric semi-rings with different radius

© 2017 г. Xia Liu**, Graduate Student; Jinping Tian*,**, Doctor of Science; Rongcao Yang**, Doctor of Science

*Computer Center of Shanxi University, Taiyuan, 030006, P. R. China
**College of Physics and Electronics Engineering of Shanxi Uni-versity, Taiyuan, 030006, P. R. China
E-mail: tianjp@sxu.edu.cn

Submitted 15.07.2017

The propagation characteristics of excited surface plasmon polaritons in a plasmonic filter are studied by controlling the geometric parameters of the waveguide. The proposed filter is composed of two nanoscale metal-insulator-metal type surface plasmon polaritons based bus waveguide connected through two face to face concentric semi-rings with different radius placed at the top and bottom sides. Numerical results show that the wavelengths of the transmission spectra dips have changes of red shift when either the radius of the two semi-rings or the refractive index of the insulator is increased. This sensitivity is superior to the filter properties, and thus we believe that the proposed waveguide structure has potential application in the nanoscale photonic devices integration.

Keywords: *surface plasmon polaritons, filter, transmission spectra.*

OCIS codes: *240.6680, 230.0230, 250.3140*

1. INTRODUCTION

The formation of surface plasmon polaritons (SPPs) is due to the interaction between the free electrons in the metal surface and the illuminated electromagnetic field. Such waves attenuate exponentially in the direction perpendicular to the interface and they can propagate along the interface over about tens micrometers or even longer. Surface plasmon polaritons have been considered as energy and information carriers in nanoscale optics owing to their ability of overcoming diffraction limit of light in conventional optical devices. Because of their potential applications to guide and manipulate light at deep subwavelength scales, SPPs are shown to be promising in highly integrated optical circuits [1–3], of which the basic structure include surface plasmon waveguides (SPWs) and filters. As an important plasmonic waveguide, the metal-insulator-metal (MIM) structures have attracted more and more attention due to their deep-subwavelength confinement of light and longer propagation length [4]. Several different MIM waveguide structures based on SPPs have been numerically and/or experimentally demonstrated, such as U-shaped waveguides [5], splitters [6], Y-shaped combiners [7], Mach-Zehnder interferometers [8], couplers [9, 10], Bragg mirrors [11], and photonic bandgap structures [12].

As one of the most prevalent devices in optical circuits, plasmonic filters based on MIM waveguide have been studied widely. Recently, some wavelength-selective and mode-selective structures have been investigated and utilized to construct plasmonic filters [13–19], including tooth-shaped filter [20–22], multichannel filter [23, 24], channel drop filter with disk resonator [25], rectangular geometry resonator [26, 27], and ring resonator [19, 28]. Recently, Wang and his coworkers [29] have investigated two-dimensional (2D) compound plasmonic structures composed of two straight MIM waveguides with a ring resonator. Their results show that some transmission resonance peaks appear at some specific wavelengths which meet the resonance conditions in the ring. The discussed compound structure in their work is symmetric with a dielectric ring working as a resonator. Therefore, a question is if the symmetrical distribution of the structure is broken, can the properties of the optical transmittance through this kind of asymmetric structure present more novel features and will the filtering performance be greatly improved?

So, in this paper, we propose a 2D-nanoscale structure which is composed of two straight MIM waveguides act as input and output waveguides, which are connected by two face-to-face concentric semi-rings with different radius. Compared with the proposed structure in this paper, most of the reported similar structures were composed of standard rings of rectangular type, circular type and also triangular type. Through the use of our new structure, one may have an additional degree of freedom over the reported standard ring structures to control the propagation properties. By adjusting the different radius of the two semi-rings, the propagation characteristics of the electromagnetic fields can be effectively controlled. These properties can be used to achieve the band selection capabilities. Due to its subwavelength scale and very simple configuration, this device can be easily fabricated and highly integrated with other micro/nano devices. Below, in Section two of this paper we will give the schematic and simulation method of the proposed filter structure and in Section three, the detail discussions of the simulation results are presented, and then in Section four we give the conclusions of the paper.

2. STRUCTURE AND METHOD

The proposed filter structure is shown in Fig. 1a. The slit widths are all denoted as $w = 50$ nm to assure that the considered electromagnetic field mode is fundamental if there are no special instructions. The inner radius of the upper semi-ring and bottom semi-ring are, respectively, r_1 and r_2. The relative permittivity of the insulator is $\varepsilon_d = n^2$, n is its

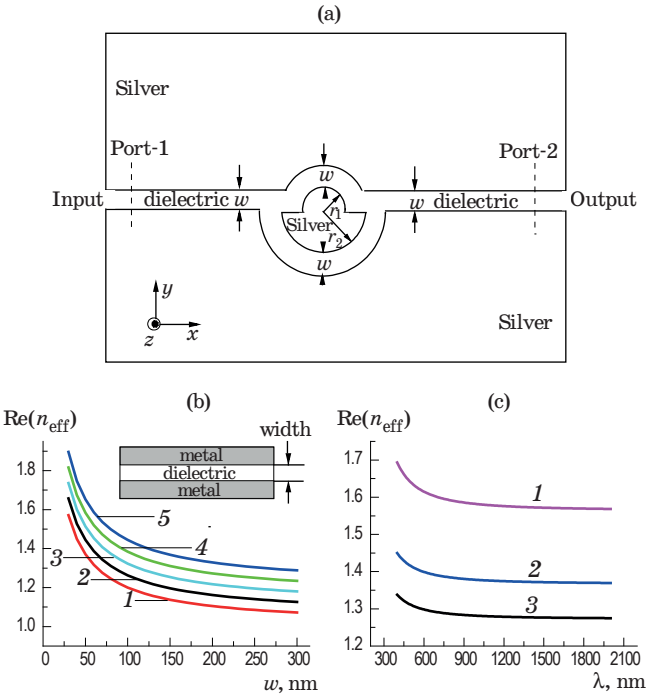

Fig. 1. (a) Schematic of the proposed filter structure. (b) Real part of the effective refractive index of an MIM waveguide versus the slit width at wavelength 1550 nm for different insulator refractive index. *1* – $n = 1$, *2* – $n = 1.05$, *3* – $n = 1.1$, 4 – $n = 1.15$, *5* – $n = 1.2$. (c) The wavelength of the incident light for different slit width. *1* – $w = 30$ nm, *2* – $w = 50$ nm, *3* – $w = 70$ nm. Inset in (b) is the basic MIM waveguide, where the insulator (white) is embedded between two silver layers (gray).

refractive index. The background material is metal silver. The frequency-dependent complex relative permittivity of silver $\varepsilon_m(\omega)$ can be given by Drude model

$$\varepsilon_m(\omega) = \varepsilon_\infty - \omega_p^2 / \omega(\omega + i\gamma), \quad (1)$$

where ε_∞ stands for the dielectric constant at the infinite frequency. γ and ω_p are the electron collision frequency and bulk plasma frequency, respectively. i is imaginary unit, ω is the angular frequency of incident light. Here we have set $\varepsilon_\infty = 3.7$, $\omega_p = 9.1$ eV, $\gamma = 0.018$ eV, according to the reported literatures [30].

The governed transverse magnetic mode dispersion equation of MIM structure can be written as [31, 32]

$$\varepsilon_d k_m + \varepsilon_m k_d \tanh((k_d/2)w) = 0, \quad (2)$$

where k_d and k_m are defined as $k_d = (\beta^2 - \varepsilon_d k_0^2)^{1/2}$, and $k_m = (\beta^2 - \varepsilon_m k_0^2)^{1/2}$. $k_0 = 2\pi/\lambda$ is the free-space wave vector. The effective refractive index of the MIM waveguide can be represented as $n_{eff} = \beta/k_0$. Eq. (2) can be solved numerically by MATLAB. The results are shown in Fig. 1b, c. It can be seen from Fig. 1b that the real part of n_{eff} is quite sensitive to the width of the insulator layer, and which will decrease as the slit width increases when the input wavelength is 1550 nm. Meanwhile, it is also found that the real part of n_{eff} will increase with the increase of the insulator's refractive index in the slit when the slit width and input wavelength are the same. Figure 1c gives the dependences of the incident light on the input wavelengths for different slit width. It can be seen that the real part of the effective refractive index also decrease gradually with the increasing of the wavelength of the incident light, and when the wavelength is larger, this change will become moderate. This result can also be verified through numerical method. Here in this paper, to investigate the transmission spectra of the proposed filter structure, the numerical simulations are carried out through the finite element method based software COMSOL with perfectly matched layer boundary conditions. The module we use is radio frequency with extreme fine mesh size in the air slit and fine mesh size in the metal cladding and substrate.

3. SIMULATIONS AND DISCUSSION

The electromagnetic fields are assumed to be incident from the left side of waveguide, and propagate along x direction. They will travel clockwise and anti-clockwise simultaneously in the upper and bottom semi-rings, and output from the right side of waveguide. Two monitors are respectively set at the locations Port-1 and Port-2 to detect the incident and transmitted field's powers P_1, P_2. Then the transmittance is defined as $T = P_2/P_1$. Simulation result illustrates that there is a transmission dip at about $\lambda = 1352$ nm when $r_1 = 100$ nm, $r_2 = 150$ nm. This result is shown in Fig. 2a. One can find that the transmission spectra exhibit a gap window with its center wavelength being about 1352 nm in which the optical pulse with the given wavelength cannot propagate. Thus it is believed that the proposed structure can act as a stop-band SPW filter. Calculation shows that the full-width at half-maximum (FWHM) is about 50 nm. In Figs. 2b–d, the distribution of electromagnetic fields at wavelength 1245, 1352 and 1490 nm are presented, and from which one can surely find that the electromagnetic field power cannot be transmitted from input to output port when input wavelength is 1352 nm. But when the wavelengths are 1245 and 1490 nm, which are far away from the stop band, the power can be well transmitted to the output port, namely, the transmitting of field power is forbidden in the case of $\lambda = 1352$ nm. Below we will study the controlling properties of this band-stop filter by adjusting the relative geometric parameters.

At first, the influence of the radius r_1 on the transmission spectra has been studied with a fixed value of $r_2 = 150$ nm. Figure 3a gives the simulation results

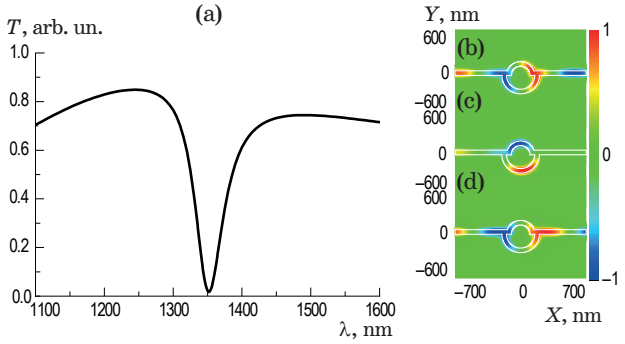

Fig. 2. (a) Transmission spectra of the proposed filter when $w = 50$ nm, $r_1 = 100$ nm and $r_2 = 150$ nm. The distribution of field component H_z is respectively shown in (b) $\lambda = 1245$ nm, (c) $\lambda = 1352$ nm, (d) $\lambda = 1490$ nm.

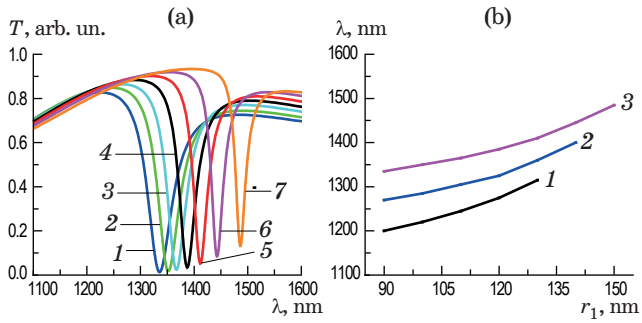

Fig. 3. (a) Transmission spectra of the proposed filter for different r_1. *1* — $r_1 = 90$ nm, *2* — $r_1 = 100$ nm, *3* — $r_1 = 110$ nm, *4* — $r_1 = 120$ nm, *5* — $r_1 = 130$ nm, *6* — $r_1 = 140$ nm, *7* — $r_1 = 150$ nm, when $r_2 = 150$ nm, $w = 50$ nm. (b) Dependences of the dip wavelengths of the transmission spectra valleys versus r_1. *1* — $r_2 = 130$ nm, *2* — $r_2 = 140$ nm, *3* — $r_2 = 150$ nm.

and as can be seen, the transmission spectra have similar shapes when r_1 changes from 90 to 150 nm. But the stop-band exhibit a trend of red shift with the increase of r_1, and this can be also valid from the results are shown in Fig. 3b which are the dependences of the transmission valleys on the value of radius r_1. In addition, the widths of the stop bands tend to be narrower when r_1 is increased. Calculation proves that the FWHM is 55 nm at $r_1 = 90$ nm and is 23 nm at $r_1 = 150$ nm. Furthermore, with the increase of r_1, the minimum transmittance will slightly increase owing to the fact that the proposed structure tends to be symmetrical which will inevitably result in some field power leaking from the input port to the output port. And due to the inevitable ohm losses, the maximal transmittance cannot reach 100%. So far, one can have a freedom to control the center wavelength of the band stop filter by adjusting r_1 but fixing the value of r_2.

Similarly, one can investigate the influence of the radius r_2 on the transmission spectra while fixing the value of r_1. As examples, Fig. 4 shows the simulation results when r_2 is increasing from 100 to 160 nm while $r_1 = 100$ nm. It can be found obviously that the transmission valleys also exhibit a red shift as the radius r_2 increases, and this is indeed in accordance with the results are shown in Fig. 3. But here the minimal values of the transmittances for different values of r_2 are almost the same due to the smaller value of both r_1 and r_2. This result also tells people that to achieve an optimal stop-band, one must make sure that the value of either r_2 or r_1 must be in a proper range to reduce the power leaking. In addition, the widths of the stop-band have a trend of broaden when r_2 is increased which is in contrary to the aforementioned case. The two results shown in Figs. 3 and 4 can be combined to prove that the narrowest width of the stop-band is obtained only when the radii of the two semi-rings are equal. Meanwhile, one can also find that the maximal values of the transmittance are always less than 100% due to the inevitable propagation losses. Figure 4b shows the dependences of the transmission valleys on the value of radius r_2.

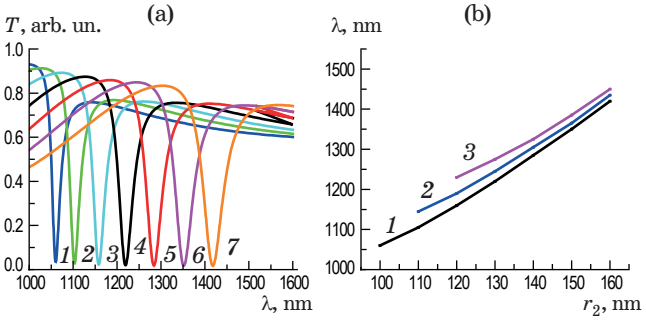

Fig. 4. (a) Transmission spectra of the proposed filter for different r_2. *1* — $r_2 = 100$ nm, *2* — $r_2 = 110$ nm, *3* — $r_2 = 120$ nm, *4* — $r_2 = 130$ nm, *5* — $r_2 = 140$ nm, *6* — $r_2 = 150$ nm, *7* — $r_2 = 160$ nm, when $r_1 = 100$ nm, $w = 50$ nm. (b) Dependences of the dip wavelengths of the transmission spectra valleys versus r_2. *1* — $r_1 = 100$ nm, *2* — $r_1 = 110$ nm, *3* — $r_1 = 120$ nm.

At second, though we have fixed the slit width as $w = 50$ nm to make the single mode transmitting in the above simulation, discussions of the influences slit width w on the transmission spectra are also necessary due to the in-laboratory manufacture error or other useful purposes. So, we have also studied the changes of the transmission spectra of the proposed filter by changing the slit width w. Figure 5a simplify shows the simulation results. It can be seen that the transmission spectra would have a blue shift when the slit width w increases from 30 to 70 nm and this can also be seen from Fig. 5b. At the same time, it is found that the width of the stop band has no clear changes when the slit width is changed. This result provides another freedom to adjusting the center wavelength of the proposed filter structure. To be noted is that one must keep the smaller value of w to make sure that the studied field mode is fundamental.

At last, it is well known that the refractive index of the insulator in the slit will play an important role in the filter processing. So, we have also carried out a round of numerical simulation by changing the

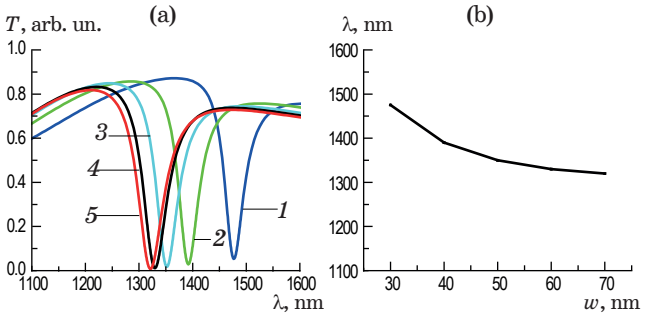

Fig. 5. (a) Transmission spectra of the proposed filter for different w. *1* — $w = 30$ nm, *2* — $w = 40$ nm, *3* — $w = 50$ nm, *4* — $w = 60$ nm, *5* — $w = 70$ nm, when $r_1 = 100$ nm, $r_2 = 150$ nm. (b) Dependences of the dip wavelengths of the transmission spectra valleys versus w.

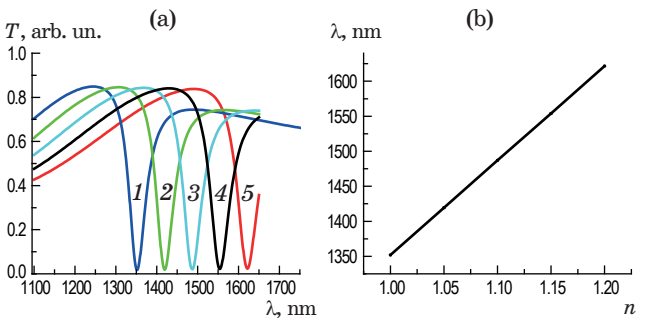

Fig. 6. (a) Transmission spectra of the proposed filter for different insulator refractive indices. *1* — $n = 1$, *2* — $n = 1.05$, *3* — $n = 1.1$, *4* — $n = 1.15$, *5* — $n = 1.2$, when $w = 50$ nm, $r_1 = 100$ nm and $r_2 = 150$ nm. (b) Dependences of the dip wavelengths of the transmission spectra valleys versus $n = (\varepsilon_d)^{1/2}$.

insulator refractive index from 1.0 to 1.2 with step of 0.05 while keeping $r_1 = 100$ nm, $r_2 = 150$ nm and $w = 50$ nm. Figure 6 shows the results. One can see that the central wavelength has a red-shift when the refractive index increases, and this change is almost linear as shown in Fig. 6b with a bigger slope. In addition, calculation results showed that the FWHM will slightly increase with the increase of insulator refractive index. This result provides one more way to control the filter central wavelength. On the other hand, it provides an application of refractive sensor to detect the material filled in the wave guide slit.

4. CONCLUSIONS

In summary, a novel SPW based filter composed of two MIM waveguide contacted by two face to face concentric MIM semi-rings with different radii is proposed. The simulation results indicate that a stop-band can be formed in the considered wavelength range, and the filter central wavelength, namely, the transmission valleys can be tuned by changing the radii of the two semi-rings, the width of the slit and the refractive index of the insulator in the slit. The proposed SPW based MIM filter structure and the studies of its propagation properties can be treated as complement of the reported SPW filter with ring resonator. We hope that the results can have potential applications in compact integrating of photonic devices and refractive index sensors.

This work was supported by the National Natural Science Foundation of China (Grant No. 61475198) and Research Project Supported by Shanxi Scholarship Council of China (Grant No. 2011-002) .

REFERENCES

1. *Barnes W.L., Dereux A., Ebbesen T.W.* Surface plasmon subwavelength optics // Nature. 2003. V. 424(6950). P. 824–830.
2. *Lezec H.J., Degiron A., Devaux E., Linke R.A., Martin-Moreno L., Garcia-Vidal F.J., Ebbesen T.W.* Beaming light from a subwavelength aperture // Science. 2002. V. 297(5582). P. 820–822.
3. *Pile D.F.P., Gramotnev D.K.* Plasmonic subwavelength waveguides: Next to zero losses at sharp bends // Opt. Lett. 2005. V. 30(10). P. 1186–1188.
4. *Leon I., Berini P.* Amplification of long-range surface plasmons by a dipolar gain medium // Nat. Photon. 2010. V. 4(6). P. 382–387.
5. *Lee T., Gray S.* Subwavelength light bending by metal slit structures // Opt. Exp. 2005. V. 13(24). P. 9652–9659.
6. *Veronis G., Fan S.* Bends and splitters in metal-dielectric-metal subwavelength plasmonic waveguides // Appl. Phys. Lett. 2005. V. 87(13). P. 131102.
7. *Gao H., Shi H., Wang C., Du C., Luo X., Deng Q., Lv Y., Lin X., Yao H.* Surface plasmon polariton propagation and combination in Y-shaped metallic channels // Opt. Exp. 2005. V. 13(26). P. 10795–10800.
8. *Wang B., Wang G.P.* Surface plasmon polariton propagation in nanoscale metal gap waveguides // Opt. Lett. 2004. V. 29(17). P. 1992–1994.
9. *Nikolajsen T., Leosson K., Bozhevolnyia S.I.* Surface plasmon polariton based modulators and switches operating at telecom wavelengths // Appl. Phys. Lett. 2004. V. 85(24). P. 5833–5835.
10. *Zhao H., Guang X., Huang J.* Novel optical directional coupler based on surface plasmon polaritons // Physica E. 2008. V. 40(10). P. 3025–3029.
11. *Dilbacher H., Krenn J.R., Schider G., Leitner A., Aussenegg F.R.* Two-dimensional optics with surface plasmon polaritons // App. Phys. Lett. 2002. V. 81(10). P. 1762–1764.
12. *Bozhevolnyi S.I., Erland J., Leosson K., Skovgaard P.M.W., Hvanm J.M.* Waveguiding in surface plasmon polariton band gap structures // Phys. Rev. Lett. 2011. V. 86(14). P. 3008–3011.
13. *Lin X.S., Huang X.G.* Tooth-shaped plasmonic waveguide filters with nanometric sizes // Opt. Lett. 2008. V. 33(23). P. 2874–2876.
14. *Zhang Z.Y., Wang J.D., Zhao Y.N., LuD., Xiong Z.H.* Numerical investigation of a branch-shaped filter based on metal-insulator-metal waveguide // Plasmonics. 2011. V. 6(4). P. 773–778.
15. *Chen P.X., Liang R.S., Huang Q.D., Yu Z., Xu X.K.* Plasmonic filters and optical directional couplers based on wide metal-insulator-metal structure // Opt. Exp. 2011. V. 19(8). P. 7633–7639.
16. *Hwang Y., Kim J.E., Park H.Y., Kee C.S.* Plasmonic stop band formation in a metal-insulator-metal ring with a narrow gap // J. Optics. 2011. V. 13(7). P. 075006.
17. *Yun B.F., Hu G. H., Cui Y.P.* Theoretical analysis of a nanoscale plasmonic filter based on a rectangular metal-insulator-metal waveguide // J. Physics D: Appl. Phys. 2010. V. 43(38) P. 385102.
18. *Zand I., Mahigir A., Pakizeh T., Abrishamian M.S.* Selective-mode optical nanofilters based on plasmonic complementary split-ring resonators // Opt. Exp. 2012. V. 20(7). P. 7516–7525.

19. *Zand I., Abrishamian M.S., Berini P.* Highly tunable nanoscale metal-insulator-metal split ring core ring resonators (SRCRRs) // Opt. Exp. 2013. V. 21(1). P. 79–86.

20. *Lin X. S., Huang X. G.* Tooth-shaped plasmonic waveguide filters with nanometric sizes // Opt. Lett. 2008. V. 33(23). P. 2874–2876.

21. *Tao J., Huang X.G., Lin X., Zhang Q., Jin X.* A narrowband subwavelength plasmonic waveguide filter with asymmetrical multiple-teeth-shaped structure // Opt. Exp. 2009. V. 17(16). P. 13989–13994.

22. *Pannipitiya A., Rukhlenko I.D., Premaratne M., Hattori H.T. Agrawal G.P.* Improved transmission model for metal-dielectric-metal plasmonic waveguides with stub structure // Opt. Exp. 2010. V. 18(6). P. 6191–6204.

23. *Luo X., Zou X.H., Li X.F, Zhou Z., Pan W., Yan L.S., Wen K.H.* High-uniformity multichannel plasmonic filter using linearly lengthened insulators in metal–insulator–metal waveguide // Opt. Lett. 2013. V. 38(9). P. 1585–1587.

24. *Wen K.H., Yan L.S., Pan W., Luo B., Guo Z., Guo Y.H., Luo X.G.* Design of plasmonic comb-like filters using loop-based resonators // Plasmonics. 2013. V. 8(2). P. 1017–1022.

25. *Lu H., Liu X.M., Mao D., Wang L.R., Gong Y.K.* Tunable band-pass plasmonic waveguide filters with nanodisk resonators // Opt. Exp. 2010. V. 18(17). P. 17922–17927.

26. *Rezaei M., Miri M., Khavasi A., Mehrany K., Rashidian B.* An efficient circuit model for the analysis and design of rectangular plasmonic resonators // Plasmonics. 2012. V. 7(2). P. 245–252.

27. *Yun B.F., Hu G.H., Cui Y.P.* Resonant mode analysis of the nanoscale surface plasmon polariton waveguide filter with rectangle cavity // Plasmonics. 2013. V. 8(2). P.267–275.

28. *Wu T.S., Liu Y.M., Yu Z.Y., Peng Y.W., Shu C.G., Ye H.* The sensing characteristics of plasmonic waveguide with a ring resonator // Opt. Exp. 2014. V. 22(7). P. 7669–7677.

29. *Wang T.B., Wen X.W., Yin C.P., Wang H.Z.* The transmission characteristics of surface plasmon polaritons in ring resonator // Opt. Exp. 2009. V. 17(26). P. 24096–24101.

30. *Johnson P.B., Christy R.W.* Optical constants of the noble metals // Phys. Rev. B. 1972. V. 6(12). P. 4370–4379.

31. *Dionne J.A., Sweatlock L.A., Atwater H.A., Polman A.* Plasmon slot waveguides: Towards chip-scale propagation with subwavelength-scale localization // Phys. Rev. B. 2006. V. 73(3). P. 035407.

32. *Wang B., Wang G.P.* Plasmon Bragg reflectors and nanocavities on flat metallic surfaces // Appl. Phys. Lett. 2005. V. 87(1). P. 013107.